

Full wave simulations of fast wave efficiency and power losses in the scrape-off layer of tokamak plasmas in mid/high harmonic and minority heating regimes

This content has been downloaded from IOPscience. Please scroll down to see the full text.

2016 Nucl. Fusion 56 016019

(<http://iopscience.iop.org/0029-5515/56/1/016019>)

View [the table of contents for this issue](#), or go to the [journal homepage](#) for more

Download details:

IP Address: 198.125.227.4

This content was downloaded on 05/01/2016 at 14:58

Please note that [terms and conditions apply](#).

# Full wave simulations of fast wave efficiency and power losses in the scrape-off layer of tokamak plasmas in mid/high harmonic and minority heating regimes\*

N. Bertelli<sup>1</sup>, E.F. Jaeger<sup>2</sup>, J.C. Hosea<sup>1</sup>, C.K. Phillips<sup>1</sup>, L. Berry<sup>3</sup>, P.T. Bonoli<sup>4</sup>, S.P. Gerhardt<sup>1</sup>, D. Green<sup>3</sup>, B. LeBlanc<sup>1</sup>, R.J. Perkins<sup>1</sup>, C.M. Qin<sup>5</sup>, R.I. Pinsker<sup>6</sup>, R. Prater<sup>6</sup>, P.M. Ryan<sup>3</sup>, G. Taylor<sup>1</sup>, E.J. Valeo<sup>1</sup>, J.R. Wilson<sup>1</sup>, J.C. Wright<sup>4</sup> and X.J. Zhang<sup>5</sup>

<sup>1</sup> Princeton Plasma Physics Laboratory, Princeton, NJ 08543, USA

<sup>2</sup> XCEL Engineering Inc., 1066 Commerce Park Drive, Oak Ridge, TN 37830, USA

<sup>3</sup> Oak Ridge National Laboratory, PO Box 2008, Oak Ridge, TN 37831-6169, USA

<sup>4</sup> Plasma Science and Fusion Center, MIT, Cambridge, MA 02139, USA

<sup>5</sup> Institute of Plasma Physics, Chinese Academy of Sciences, Hefei 230031, People's Republic of China

<sup>6</sup> General Atomics, PO Box 85608, San Diego, CA 92186-5608, USA

E-mail: [nbertell@pppl.gov](mailto:nbertell@pppl.gov)

Received 26 August 2015, revised 4 November 2015

Accepted for publication 13 November 2015

Published 17 December 2015



CrossMark

## Abstract

Several experiments on different machines and in different fast wave (FW) heating regimes, such as hydrogen minority heating and high harmonic fast waves (HHFW), have found strong interaction between radio-frequency (RF) waves and the scrape-off layer (SOL) region. This paper examines the propagation and the power loss in the SOL by using the full wave code AORSA, in which the edge plasma beyond the last closed flux surface (LCFS) is included in the solution domain and a collisional damping parameter is used as a proxy to represent the real, and most likely nonlinear, damping processes. 2D and 3D AORSA results for the National Spherical Torus eXperiment (NSTX) have shown a strong transition to higher SOL power losses (driven by the RF field) when the FW cut-off is removed from in front of the antenna by increasing the edge density. Here, full wave simulations have been extended for 'conventional' tokamaks with higher aspect ratios, such as the DIII-D, Alcator C-Mod, and EAST devices. DIII-D results in HHFW regime show similar behavior found in NSTX and NSTX-U, consistent with previous DIII-D experimental observations. In contrast, a different behavior has been found for C-Mod and EAST, which operate in the minority heating regime.

Keywords: fast wave, heating losses, scrape-off layer, HHFW, ICRH, SOL, power losses

(Some figures may appear in colour only in the online journal)

## 1. Introduction

In fusion experiments, fast wave (FW) heating in the ion cyclotron range of frequency (ICRF) has been successfully used to sustain and control the plasma performance.

\* This article is dedicated to the memory of Cynthia K. Phillips

Consequently, ICRF heating is planned to play an important role in the ITER experiment [1]. However, the understanding of the interaction between ICRF antennas and the scrape-off layer (SOL) plasma is crucial in order to optimize the performance of ICRF in a tokamak. In fact, many ICRF heating experiments [2–9] have found regimes in which significant

fractions of the coupled RF power does not appear in the plasma core. Experimental studies on erosion and impurity generation in the presence of ICRF have been performed on different machines [4, 7–10], showing that SOL RF losses are indeed an important contribution to these effects. In the recent years, a large effort has been made to understand the main physical mechanisms behind the interaction between RF waves and the SOL, such as parametric decay [3, 11–13], sheath effects [14, 15], etc. Recently, experimental studies employing high harmonic fast wave (HHFW) heating on the National Spherical Torus eXperiment (NSTX) [16], a low aspect ratio tokamak, have shown that substantial HHFW power loss (up to 60% of the HHFW power coupled from the antenna) can occur along the open field lines in the SOL [6, 17–20].

This paper examines FW power loss in the SOL by using the numerical full wave simulation code AORSA [21], in which the edge plasma beyond the last closed flux surface (LCFS) is included in the solution domain [22]. The AORSA code includes, throughout the plasma, the standard kinetic effects, such as the Landau damping and the transit-time magnetic pumping (TTMP), in the hot plasma dielectric tensor. Additionally, here a collisional damping parameter is used as a proxy to represent the real, and most likely nonlinear, damping processes [23, 24] in order to predict the effects, and possible causes, of the power loss in the SOL. In [24], AORSA simulations with a single dominant mode number and several toroidal mode numbers have shown a direct correlation between the location of the fast wave cut-off layer, the large amplitude of the RF fields in the scrape-off region, and the power losses in the SOL (driven by the RF field) observed in the NSTX experiments. More specifically, a large electric field in the SOL is found when the FW propagates in the SOL at increased SOL density.

An extension of these simulations to other devices with different geometries and FW heating regimes is performed in order to explain the prediction of AORSA in the SOL plasma for a wide range of ICRF. In particular numerical simulations are applied to ‘conventional’ tokamaks with higher aspect ratios, such as DIII-D [25], Alcator C-Mod [26] and EAST [27]. It is important to note that the FW heating regime adopted in DIII-D is a mid/high harmonic regime (similar to the NSTX-U [28] heating regime at full toroidal field), which differs from the, more common, minority heating regime adopted in EAST and Alcator C-Mod.

This paper is structured as follows: in section 2 a brief introduction of the full wave AORSA code together with 2D AORSA results (obtained with a single toroidal mode) are presented for NSTX and NSTX-U. Also, a sensitivity analysis on the proxy collisional damping is presented and discussed. Full wave simulations applied to ‘conventional’ tokamaks, such as DIII-D, Alcator C-Mod, and EAST are shown in section 3 together with a sensitivity analysis of the proxy collisional damping for each device. In section 4, a discussion on the simulation results obtained for different fast wave heating regimes is presented in terms of the pitch angle of the magnetic field, the hydrogen minority ICRF versus mid/high

harmonic ICRH regimes. Finally, the main conclusions of the work are summarized in section 5.

## 2. AORSA results for NSTX

AORSA is a full wave code that solves the Helmholtz wave equation for a tokamak geometry, including the SOL region beyond the LCFS where the magnetic field lines are open [21, 22]. The density profile adopted in the SOL is given by

$$n_e = n_{\text{ant}} + [n_e(\rho = 1) - n_{\text{ant}}] \exp\left[\frac{\rho - 1}{d_{\text{SOL}}}\right], \quad \rho \geq 1 \quad (1)$$

where an exponential decay is prescribed from the LCFS,  $n_{\text{ant}}$  is the minimum electron density just in front of the antenna,  $\rho$  is the square root of the normalized poloidal flux, and  $d_{\text{SOL}}$  is a SOL decay length.  $n_{\text{ant}}$  and  $d_{\text{SOL}}$  are input to AORSA and they can be modified in order to fit as best as possible the experimental data [22, 24]. Within the LCFS, the density profile is obtained from measurements. Furthermore, AORSA is valid for ‘all orders’ retaining all contributions in  $k_{\perp}\rho_i$  ( $k_{\perp}$  and  $\rho_i$  are the perpendicular component of the wave vector relative to the local equilibrium magnetic field and the ion Larmor radius, respectively) and the harmonic number. The electric field in AORSA is implemented as a Fourier decomposition in the Cartesian coordinates  $x$  and  $y$  (in the poloidal plane) and in the toroidal direction of symmetry ( $\phi$ ):

$$E(x, y, \phi) = \sum_{n_{\phi}} \sum_{n, m} E_{n_{\phi}, n, m} e^{in_{\phi}\phi} e^{k_n x + k_m y} \quad (2)$$

where  $x = R - R_0$  ( $R$  and  $R_0$  are the radial coordinate and the major radius, respectively),  $y$  is the vertical distance from the midplane,  $n_{\phi}$  is the toroidal mode number, and  $n, m$  are the Fourier mode numbers. AORSA can be run by using the single dominant toroidal mode number,  $n_{\phi}$ , of the antenna spectrum for a specific antenna phasing (in this paper, we will refer to this as 2D AORSA results) or by using the full antenna spectrum summing over several toroidal mode numbers with toroidal mode spectral weightings calculated for a specific antenna phasing (in this paper, we will refer to this as 3D AORSA results), as shown in [24]. Moreover, the full hot plasma dielectric tensor implemented in AORSA includes the standard Landau damping and the TTMP kinetic effects. Finally, in order to estimate the power lost to the SOL, an artificial ‘collisional’ damping mechanism has been implemented in AORSA as a proxy to represent the actual mechanism(s) which is(are) presently unknown [23, 24]. A collisional frequency,  $\nu$ , has been implemented as the imaginary part of the angular frequency,  $\omega$ , in the argument of the Plasma Dispersion function [23, 24]. The term  $\nu/\omega$  is an AORSA input parameter and allows us to estimate the power losses in the SOL region and, more specifically, their behavior as a function of the density in front of the antenna. It is worth recalling that without adding a proxy damping mechanism in the SOL, such as the collisional damping adopted here, no significant SOL power losses are predicted in the simulations, even in the presence of a large total electric field amplitude in the SOL and the standard kinetic effects in the dielectric

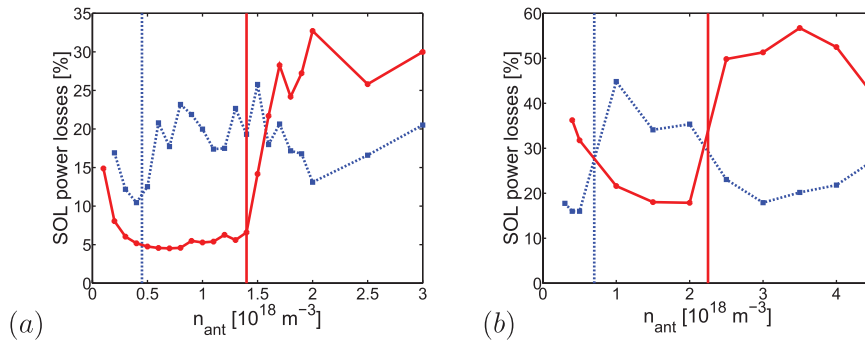


**Figure 1.** Fraction of power lost to the SOL as a function of the density in front of the antenna for  $n_\phi = -21$  (solid curve) and  $n_\phi = -12$  (dashed curve), for an NSTX case (shot 130 621) with  $B_T = 0.55$  T (figure (a)) and NSTX-U case with  $B_T = 0.76$  T (figure (b)). The vertical lines represent the value of the density for which the FW can propagate in the SOL.

tensor (see also [24]). Figure 1 recalls similar results presented in [24] but for a different NSTX shot, i.e. 130 621 with  $n_{e,0} = 2.7 \times 10^{19} \text{ m}^{-3}$ ,  $T_{e,0} = 1.2$  keV, and  $B_0 = 0.55$  T (figure (a)) and a NSTX-U case with  $n_{e,0} = 1.2 \times 10^{20} \text{ m}^{-3}$ ,  $T_{e,0} = 1.1$  keV, and  $B_0 = 0.76$  T (figure (b)), assuming a single dominant mode corresponding to the antenna phase considered. The wave frequency is 30 MHz. These figures show the predicted fraction of power absorbed in the SOL region (SOL power losses) as a function of the density in front of the antenna ( $n_{\text{ant}}$ ) assuming  $\nu/\omega = 0.01$ . Two different antenna phases are shown:  $n_\phi = -12$  (dashed curve) and  $-21$  (solid curve). The vertical lines represent the density at which the wave is propagating in front of the antenna. As shown in figure 2 of [24], the amplitude of the electric field starts to increase in the SOL region as  $n_{\text{ant}}$  increases beyond this cutoff value. This density is associated with the FW wave cut-off (the right-hand cut-off), which for a single ion species plasma and  $\omega < |\omega_{ce}|$  ( $\omega_{ce}$  is the electron cyclotron angular frequency), can be written as [6, 17, 24]

$$n_{e, \text{FW cut-off}} \propto \frac{k_{\parallel}^2 B}{\omega}, \quad (3)$$

where  $k_{\parallel}$  and  $B$  are the parallel component of the wave vector and the equilibrium magnetic field, respectively. From these figures, a clear correlation between the location of the fast wave cut-off and the RF power losses in the SOL is found in NSTX and NSTX-U as observed in [24]. More specifically, (i) when the wave can propagate in the SOL the electric field outside of LCFS significantly increases (see figure 2 in [24], where no collisional damping is added); (ii) when evanescent waves become propagating waves in the SOL, due to higher density in front of the antenna, the power losses start to increase significantly, commensurate with the amplitude of the RF field found in the SOL; (iii) for lower  $n_\phi$  ( $n_\phi/R = k_\phi \sim k_{\parallel}$ ) the transition, from low to high SOL power losses, occurs at lower  $n_{\text{ant}}$  and for higher  $B$  the transition occurs at higher  $n_{\text{ant}}$ , clearly following equation (3). For very low density the RF power losses tend to increase again with decreasing density, due to the fact that the wave is so strongly evanescent that the power can only be damped in front of the antenna, consistent with the large electric field localized in front of the antenna (as indicated in figures 1(a) and (b)). In addition, the 3D AORSA results, where the full antenna spectrum is

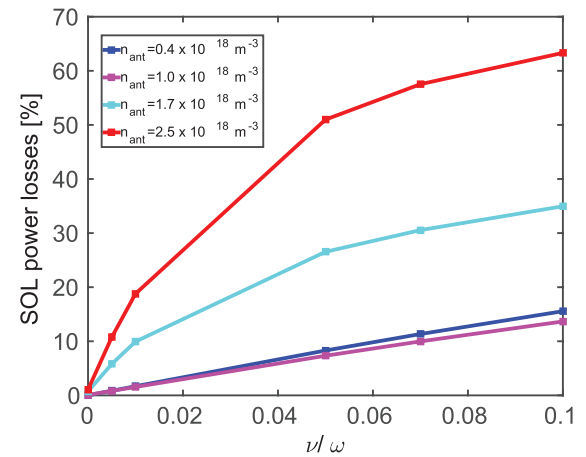


**Figure 2.** Fraction of power lost to the SOL as a function of  $\nu/\omega$  for four different values of  $n_{\text{ant}} = 0.4 \times 10^{18} \text{ m}^{-3}$ ,  $1.0 \times 10^{18} \text{ m}^{-3}$ ,  $1.7 \times 10^{18} \text{ m}^{-3}$ , and  $2.5 \times 10^{18} \text{ m}^{-3}$  with  $n_\phi = -21$  for NSTX shot 130 608 as previously shown in [24].

reconstructed, exhibit similar behavior to that of the dominant mode (2D) runs and, in particular reproduce a similar transition in SOL power losses as a function of the density in front of the antenna [24]. Before extending our 2D AORSA simulations to tokamaks with ‘conventional’ geometry and also different heating regimes, a sensitivity analysis for the  $\nu/\omega$  parameter for a NSTX case is shown in figure 2. In [24] and in figure 1, a fixed value of  $\nu/\omega$  was adopted in the numerical simulations whereas figure 2 shows a scan in  $\nu/\omega$  for four different values of  $n_{\text{ant}} = 0.4 \times 10^{18} \text{ m}^{-3}$ ,  $1.0 \times 10^{18} \text{ m}^{-3}$ ,  $1.7 \times 10^{18} \text{ m}^{-3}$ , and  $2.5 \times 10^{18} \text{ m}^{-3}$  with  $n_\phi = -21$  for NSTX shot 130 608. From this figure one can see that for the two low  $n_{\text{ant}}$  values (where FW is evanescent in the SOL) low fractions of power lost to the SOL are found while for two high  $n_{\text{ant}}$  (where FW is propagating in the SOL) values higher fractions of power lost to the SOL are found for all  $\nu/\omega$  values in agreement with the results shown in [24]. Therefore the general behavior of the fraction of power lost to the SOL does not change varying the  $\nu/\omega$  values. One can also note that the case for  $n_{\text{ant}} = 0.4 \times 10^{18} \text{ m}^{-3}$  has larger fraction of power lost to the SOL with respect to the case for  $n_{\text{ant}} = 1.0 \times 10^{18} \text{ m}^{-3}$  for the reason mentioned above: decreasing the density at very low values, the amplitude of electric field in the SOL is strongly localized and increased in front of the antenna and

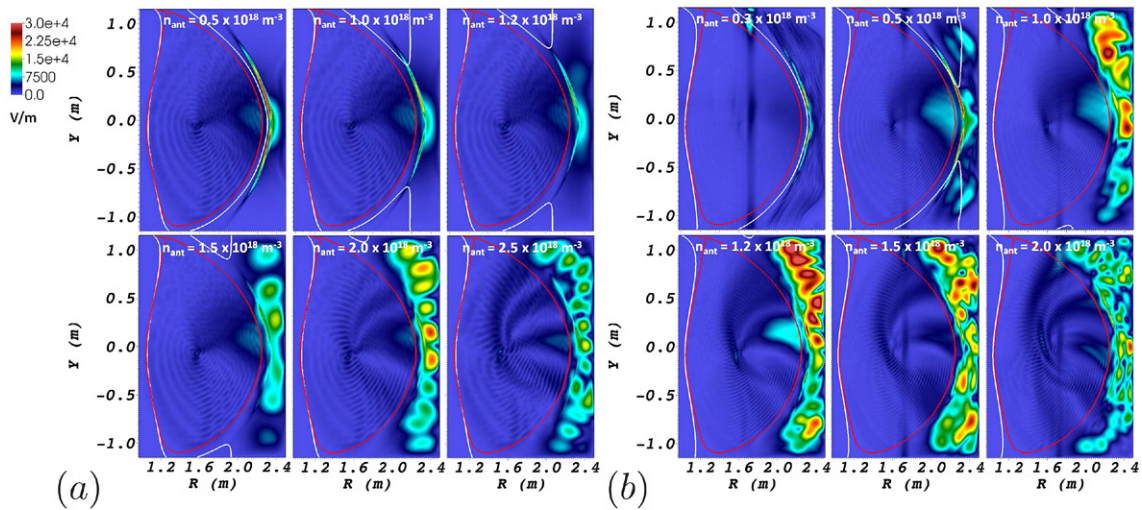


**Figure 3.** Total electric field amplitude for different density values in front of the antenna ( $n_{\text{ant}}$ ) (shown in the plots) with toroidal mode numbers  $n_{\phi} = 15$  and  $\omega/2\pi = 60$  MHz (a) and  $\omega/2\pi = 90$  MHz (b), for DIII-D shot 111 221. The white and red curves indicate the FW cut-off layer and the LCFS, respectively.

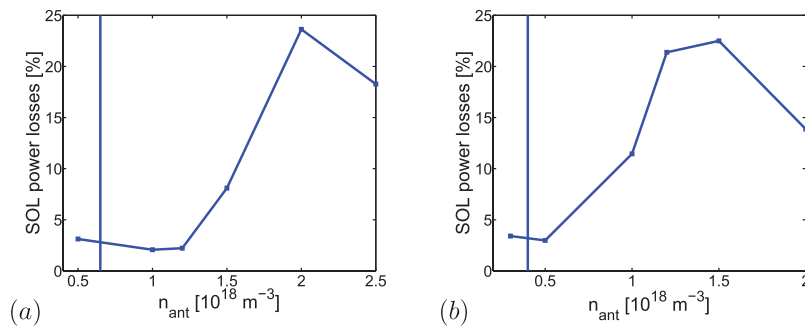


**Figure 4.** Fraction of power lost to the SOL as a function of the density in front of the antenna for  $\omega/2\pi = 60$  MHz (a) and  $\omega/2\pi = 90$  MHz (b) with  $n_{\phi} = 15$  for DIII-D shot 111 221. The vertical lines represent the value of the density for which the FW cut-off starts to be ‘open’ in front of the antenna (see figures 3(a) and (b)).

therefore the power losses tend to increase again (see figure 3 in [24] and figure 1 in this paper).

2D AORSA simulations to tokamaks with ‘conventional’ geometry and also different heating regimes are presented and discussed in the following section.

### 3. Numerical simulations on DIII-D, C-Mod, and EAST devices

We extend the numerical simulations to ‘conventional’ tokamaks with higher aspect ratios, such as DIII-D, C-Mod, and EAST devices, in order to estimate the behavior of the RF power losses in ‘standard’ tokamak geometry experiments and compare them with NSTX/NSTX-U results. Note that FW experiments in DIII-D are in the mid/high harmonic regime [29], while in C-Mod and EAST they are in the minority heating regime [8, 30].

#### 3.1. DIII-D results

FW current drive experiments in DIII-D used frequencies of  $\omega/2\pi = 60$ –120 MHz and the range of toroidal fields of

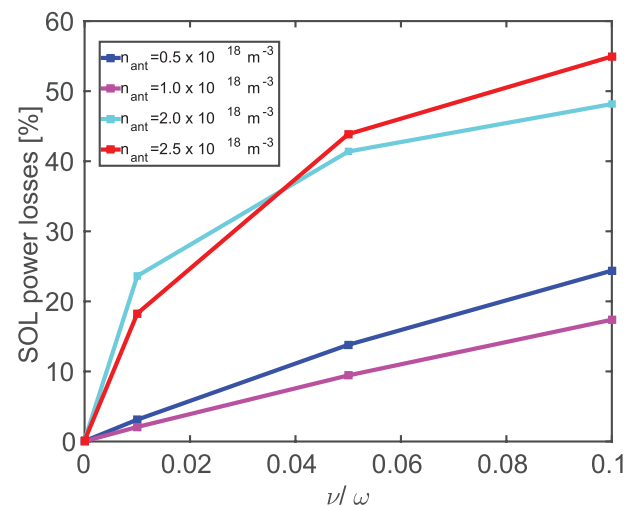


**Figure 5.** Fraction of power lost to the SOL as a function of  $\nu/\omega$  for four different values of  $n_{\text{ant}} = 0.5 \times 10^{18} \text{ m}^{-3}$ ,  $1.0 \times 10^{18} \text{ m}^{-3}$ ,  $2.0 \times 10^{18} \text{ m}^{-3}$ , and  $2.5 \times 10^{18} \text{ m}^{-3}$  with  $\omega/2\pi = 60$  MHz and  $n_{\phi} = 15$  for DIII-D shot 111 221.

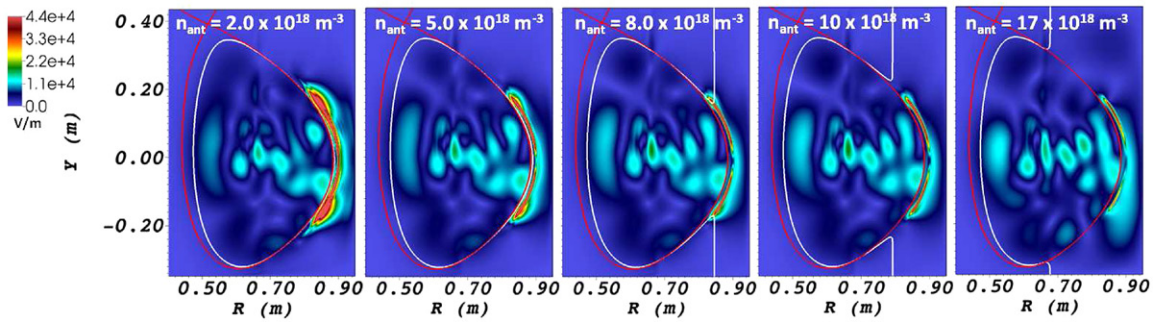


**Figure 6.** Total electric field amplitude for different density values in front of the antenna ( $n_{\text{ant}}$ ) (shown in the plots) with toroidal mode numbers  $n_{\phi} = 10$  and  $\omega/2\pi = 80$  MHz, for Alcator C-Mod. The white and red curves indicate the FW cut-off layer and the LCFS, respectively.

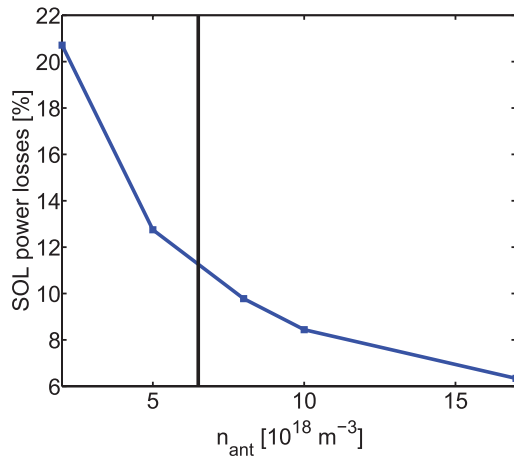


**Figure 7.** Fraction of power lost to the SOL as a function of the density in front of the antenna with for  $n_{\phi} = 10$  for Alcator C-Mod case. The vertical line represents the value of the density for which the FW cut-off starts to be ‘open’ in front of the antenna.

$B_T = 1.3\text{--}2.1$  T, therefore the FW heating scheme is in the mid/high harmonic regime ( $\omega/\omega_{c,D} = 4\text{--}12$ , where  $\omega_{c,D}$  is the deuterium angular cyclotron frequency) [29], which is similar to the regime adopted in NSTX/NSTX-U. Previous experimental work on DIII-D found a clear reduction of the FW current drive efficiency in the core due to an increase in the edge losses as the SOL density was increased above the FW cut-off [2]. For this reason, a 2D AORSA numerical analysis has been performed for a DIII-D case. Figure 3 shows the total electric field amplitude for DIII-D shot 111 221 ( $n_{e,0} = 6.1 \times 10^{19} \text{ m}^{-3}$ ,  $T_{e,0} = 4.4$  keV, and  $B = 1.85$  T) with  $n_{\phi} = 15$  for  $\omega/2\pi = 60$  MHz (figure 3(a)) and  $\omega/2\pi = 90$  MHz (figure 3(b)). For both cases, the strong increase of the total electric field amplitude occurs when the wave can propagate outside the LCFS as found in the NSTX and NSTX-U numerical analysis. The corresponding SOL power losses are shown in figure 4 for  $\nu/\omega = 0.01$  and both frequency values. We clearly see the same transition found in the results shown for NSTX/NSTX-U. In addition, for higher  $\omega/2\pi$  the transition occurs at lower  $n_{\text{ant}}$  as expected from equation (3). Moreover, these results are in agreement with previous DIII-D experimental observation [2], pointing out the importance of the location of the FW cut-off and the associated SOL density. A difference between the NSTX and DIII-D cases should be noted: in the latter case the

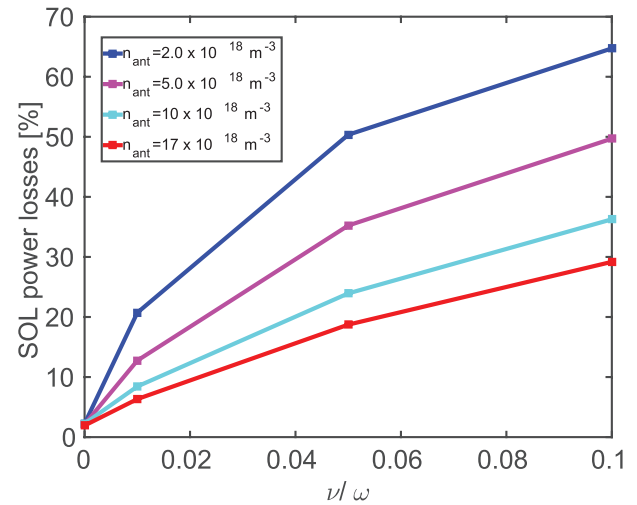


**Figure 8.** Fraction of power lost to the SOL as a function of  $\nu/\omega$  for four different values of  $n_{\text{ant}} = 2.0 \times 10^{18} \text{ m}^{-3}$ ,  $5.0 \times 10^{18} \text{ m}^{-3}$ ,  $10 \times 10^{18} \text{ m}^{-3}$ , and  $17 \times 10^{18} \text{ m}^{-3}$  with  $\omega/2\pi = 80$  MHz and  $n_{\phi} = 10$  for Alcator C-Mod case.

standing wave does not appear as soon as the cut-off is ‘open’ in front of the antenna as found in NSTX (see also discussion on pitch angle in section 4.1). Figure 5 shows the fraction of power lost to the SOL as a function of  $\nu/\omega$  for four different values of  $n_{\text{ant}} = 0.5 \times 10^{18} \text{ m}^{-3}$ ,  $1.0 \times 10^{18} \text{ m}^{-3}$ ,  $1.7 \times 10^{18} \text{ m}^{-3}$ , and  $2.5 \times 10^{18} \text{ m}^{-3}$  with  $\omega/2\pi = 60$  MHz and  $n_{\phi} = 15$ . For the two low (high) density values, where FW is evanescent (propagating) in the SOL, we found low (high) fraction of power lost to the SOL (see also figure 4(a)) in agreement with the NSTX results shown in figure 2.

### 3.2. Alcator C-Mod results

As mentioned above, ion cyclotron resonance heating (ICRH) of the hydrogen-minority species in a deuterium majority plasma is the prime auxiliary heating scheme on Alcator C-Mod [8], which differs from the mid/high harmonic regime adopted in DIII-D and NSTX/NSTX-U. Figure 6 shows the total electric field amplitude for Alcator C-Mod with  $\omega/2\pi = 80$  MHz for  $n_{\phi} = 10$  and the different values of  $n_{\text{ant}}$  shown in the plots. The central electron density and temperature are  $n_{e,0} = 1.3 \times 10^{20} \text{ m}^{-3}$ ,  $T_{e,0} = 3.6$  keV, respectively.

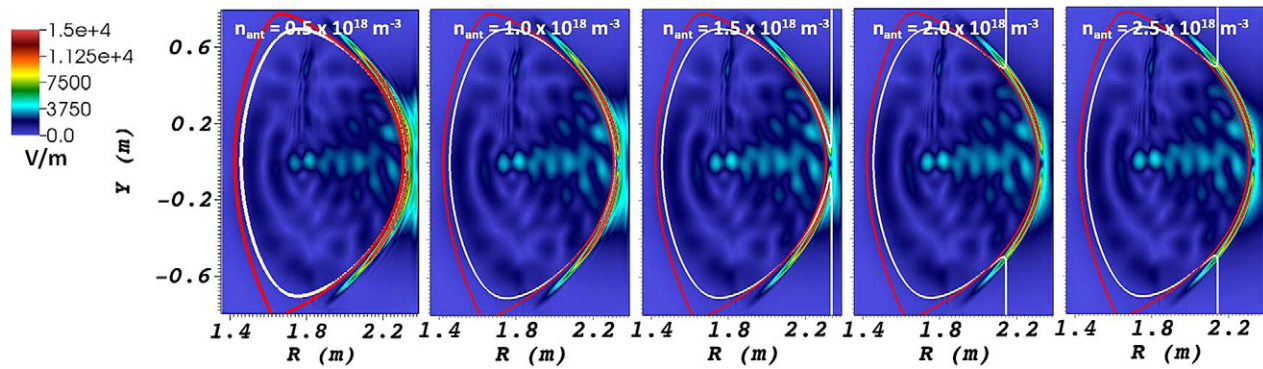


**Figure 9.** Total electric field amplitude for different density values in front of the antenna ( $n_{\text{ant}}$ ) (shown in the plots) with toroidal mode numbers  $n_\phi = 12$  and  $\omega/2\pi = 27$  MHz, for EAST shot 36 217. The white and red curves indicate the FW cut-off layer and the LCFS, respectively.

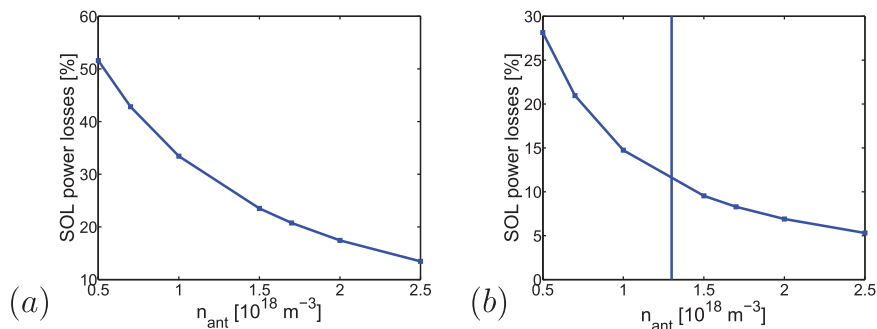


**Figure 10.** Fraction of power lost to the SOL as a function of the density in front of the antenna with for  $n_\phi = 23$  (a) and  $n_\phi = 12$  (b) for EAST discharge 36 217. The vertical line in figure (a) represents the value of the density for which the FW cut-off starts to be ‘open’ in front of the antenna.

In this figure, one can note that, unlike NSTX/NSTX-U and DIII-D, the total electric field amplitude decreases outside of LCFS with increasing  $n_{\text{ant}}$ , even when the wave can propagate in the SOL. Figure 7 shows the SOL power losses as a function of  $n_{\text{ant}}$  evaluated for  $\nu/\omega = 0.01$ . The behavior of the SOL power losses shown in figure 7 is clearly different to the behavior shown in figure 1 for NSTX/NSTX-U, and figure 4 for DIII-D; in other words, in Alcator C-Mod the transition to higher SOL power losses does not appear with increasing  $n_{\text{ant}}$ . A sensitivity scan on  $\nu/\omega$  is shown in figure 8 where the fraction of power lost to the SOL is plotted as a function of  $\nu/\omega$  for different values of  $n_{\text{ant}}$ . From this figure one can note that for all  $\nu/\omega$  values the fraction of the power lost to the SOL decreases with increasing  $n_{\text{ant}}$  unlike the NSTX/NSTX-U and DIII-D results.

Section 5 presents a discussion of some elements that might contribute to the differences mentioned above.

### 3.3. EAST results

The heating scheme in EAST is the same hydrogen minority heating used in Alcator-C-Mod [30]. To have a wide comparison between different devices, we follow the same exercise performed for NSTX/NSTX-U, DIII-D, and Alcator C-Mod. Figure 9 shows the total electric field amplitude for EAST shot 36 217 ( $n_{e,0} = 5.6 \times 10^{19} \text{ m}^{-3}$ ,  $T_{e,0} = 2.1 \text{ keV}$ ) with  $\omega/2\pi = 27$  MHz for  $n_\phi = 12$  for different values of  $n_{\text{ant}}$ .

Although the ‘standard’ dominant toroidal mode in EAST is  $n_\phi = 23$ , we chose  $n_\phi = 12$  in order to study the behavior of the SOL power losses with and without an evanescent layer in front of the antenna for this specific EAST shot as was done for the NSTX/NSTX-U, DIII-D, and Alcator C-Mod cases. In figure 9, one can note that, unlike NSTX/NSTX-U and DIII-D but like Alcator C-Mod, the total electric field amplitude does not increase outside of LCFS with increasing  $n_{\text{ant}}$ , even when the wave can propagate in the SOL. Figure 10 shows the SOL power losses as a function of  $n_{\text{ant}}$  for  $n_\phi = 23$  (figure 10(a)) and  $n_\phi = 12$  (figure 10(b)) evaluated for  $\nu/\omega = 0.01$ . Note that unlike figure 10(b), in figure 10(a) the wave is always evanescent in the SOL for the given density range. The behavior of the SOL power losses shown in figure 10 is similar to Alcator C-Mod results and is different to the NSTX/NSTX-U and DIII-D results. As shown for the previous cases, figure 11 shows the fraction of power lost to the SOL as a function of  $\nu/\omega$  for different values of  $n_{\text{ant}}$ . From this figure one can see that the SOL power losses behave in the same way as found in Alcator C-Mod independent of the value of  $\nu/\omega$  adopted, namely, for a given  $\nu/\omega$  value the SOL power losses decrease with increasing  $n_{\text{ant}}$ .

Both in Alcator C-Mod and EAST, we have found something perhaps more intuitive with respect to the NSTX/NSTX-U and DIII-D results: the increase of the SOL density enhances the antenna-plasma coupling and, as a consequence, we get a lower fraction of power lost to the SOL region.

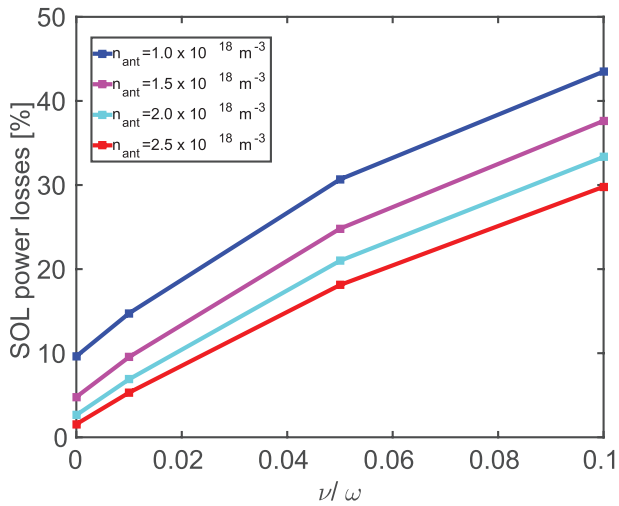


**Figure 11.** Fraction of power lost to the SOL as a function of  $\nu/\omega$  for four different values of  $n_{\text{ant}} = 1.0 \times 10^{18} \text{ m}^{-3}$ ,  $1.5 \times 10^{18} \text{ m}^{-3}$ ,  $2.0 \times 10^{18} \text{ m}^{-3}$ , and  $2.5 \times 10^{18} \text{ m}^{-3}$  with  $\omega/2\pi = 27 \text{ MHz}$  and  $n_{\phi} = 12$  for EAST case.

In the following section, we discuss some aspects that might contribute to generating different behaviors in the fraction of power lost to the SOL region for different FW regimes and devices, as found in the AORSA full wave simulations.

#### 4. Discussion

The full wave numerical simulations presented here show two different behaviors of the fraction of power lost to the SOL region: (i) for mid/high harmonic ICRH regime, as in NSTX/NSTX-U and DIII-D, high density in front of the antenna, although positive for the antenna-plasma coupling (the antenna-plasma coupling is poor (good) for low (high) density in front of the antenna), leads to an increase of the RF electric field in the SOL and corresponding increased RF power losses; (ii) for the hydrogen minority heating regime, as in Alcator C-Mod and EAST, the RF electric field is more localized at the front of the antenna, but more importantly, SOL power losses decrease with increasing density in front of the antenna. The former is in agreement with the experimental observations found in NSTX [6, 17–20] and DIII-D [2]. The latter is consistent with the fact that a higher SOL density results in a higher antenna-plasma coupling and lower SOL power losses. This aspect is in agreement with ICRH minority heating experiment in the ICRF minority heating experiments [9, 10, 31–33] although additional experimental studies might be required for quantitative comparison. Recently, NSTX experiments have shown that HHFW power lost to the SOL flows from the NSTX antenna region to the hot spots in divertor region essentially along field lines [19, 20]. In Alcator C-Mod strong ICRF-enhanced plasma potentials have been observed in the SOL regions that are not magnetically mapped to the active ICRF antennas [34]. Additional and systematic experimental measurements dedicated to the study of the interaction between the HHFW antenna and SOL region in the upcoming NSTX-U

**Table 1.** Magnetic field on axis,  $B_{T,0}$ , plasma current,  $I_p$ , and the flux surface averaged of magnetic field pitch at  $\rho = 1$  ( $\langle B_p/B_T \rangle(\rho = 1)$ ) for different devices used in this paper.

	NSTX	NSTX-U	DIII-D	C-Mod	EAST
$B_{T,0}$ [T]	0.55	1	1.85	5.41	1.95
$I_p$ [MA]	1	1	1.2	1	0.49
$\langle B_p/B_T \rangle(\rho = 1) \sim$	0.34	0.19	0.12	0.10	0.08

campaign are necessary for more quantitative evaluation and will be carried out in order to better understand the physical mechanism(s) behind the RF power lost to the SOL in comparison to other machines. Moreover, such experimental measurements will be very important to validate the AORSA full wave simulations. A common conclusion that can be drawn from these numerical results for different devices and heating regimes is that the values and the behavior of the density in front of the antenna are crucial for improving RF performance and the optimization of the density in the SOL is essential.

In the following two subsections we explore and discuss some aspects that can contribute to generating differences in the behavior of the RF field amplitude and the corresponding RF power in the SOL region for the ICRF regimes commented above.

##### 4.1. Pitch angle of the magnetic field

A distinct element that differs between the devices analyzed in this work is the magnetic field pitch angle. The spherical tokamak, such as NSTX/NSTX-U, has a large pitch angle due to a large plasma current and a low magnetic field with respect to the ‘conventional’ tokamak. Table 1 shows the value of the magnetic field on the magnetic axis, the plasma current, and the flux surface averaged of the ratio of the poloidal and toroidal magnetic field at  $\rho = 1$  ( $\langle B_p/B_T \rangle(\rho = 1)$ ) for NSTX, NSTX-U, DIII-D, Alcator C-Mod, and EAST as indicated in the equilibrium files (‘geqsk’ file) used in the numerical simulations. As expected, from this table it is seen that Alcator C-Mod and EAST have a smaller magnetic field pitch angle with respect to NSTX, NSTX-U, and a somewhat smaller pitch angle with respect to DIII-D. It is important to note that between NSTX and NSTX-U and between NSTX-U and DIII-D there is a significant difference in the value of the pitch angle as shown by  $\langle B_p/B_T \rangle(\rho = 1)$  in table 1. More specifically, there is almost a factor 3 in the flux surface averaged of magnetic field pitch between NSTX and DIII-D. Nonetheless, AORSA simulations, presented in this work, show similar results between these two cases (see sections 2 and 3.1) which would suggest that the pitch angle does not have a significant effect on the simulations. In order to further explain the effect of the magnetic field pitch angle has on the behavior of the RF electric field and the associated power lost in the SOL, different NSTX-U magnetic equilibria have been generated by the stand-alone free-boundary equilibrium ISOLVER code (some information on this code can be found in [35]) for  $B_{T,0} = 1 \text{ T}$  and  $I_p = 0.5, 1.0, 1.6,$  and  $2 \text{ MA}$ . Figure 12 shows the amplitude of the RF electric field for these cases with  $n_{\phi} = -21$  and  $n_{\text{ant}} = 5.0 \times 10^{18} \text{ m}^{-3}$ , a density at which

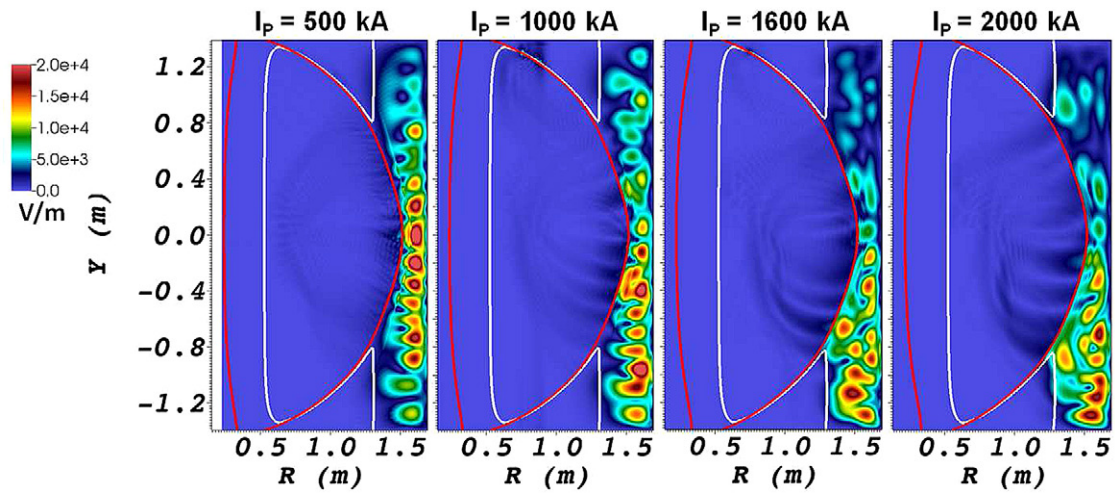


**Figure 12.** Total electric field amplitude for different NSTX-U equilibria (generated by ISOLVER) with toroidal mode numbers  $n_\phi = -21$ ,  $B_T = 1$  T, different plasma currents (shown in the plots), and  $n_{\text{ant}} = 5 \times 10^{18} \text{ m}^{-3}$ . The white and red curves indicate the FW cut-off layer and the LCFS, respectively.

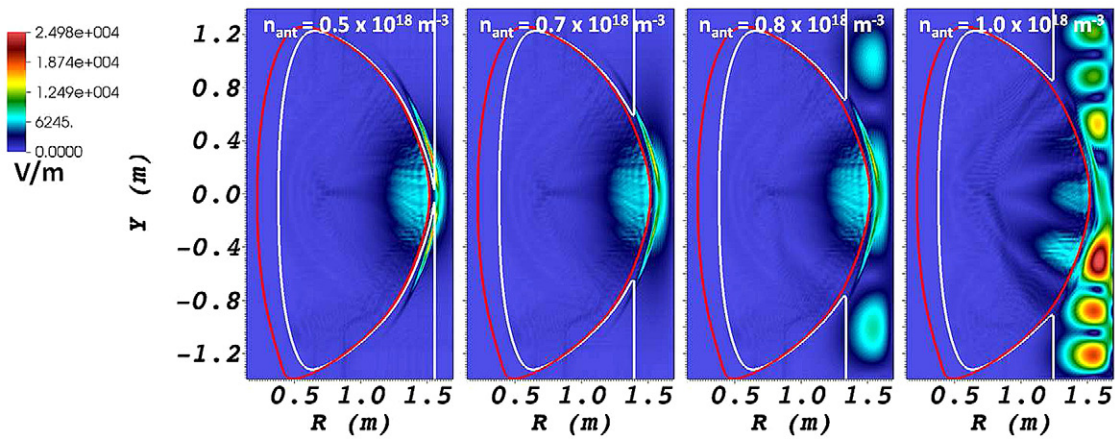


**Figure 13.** Total electric field amplitude for different density values in front of the antenna ( $n_{\text{ant}}$ ) (shown in the plots) with toroidal mode numbers  $n_\phi = -12$  and purely toroidal magnetic field for NSTX shot 130 608. The white and red curves indicate the FW cut-off layer and the LCFS, respectively.

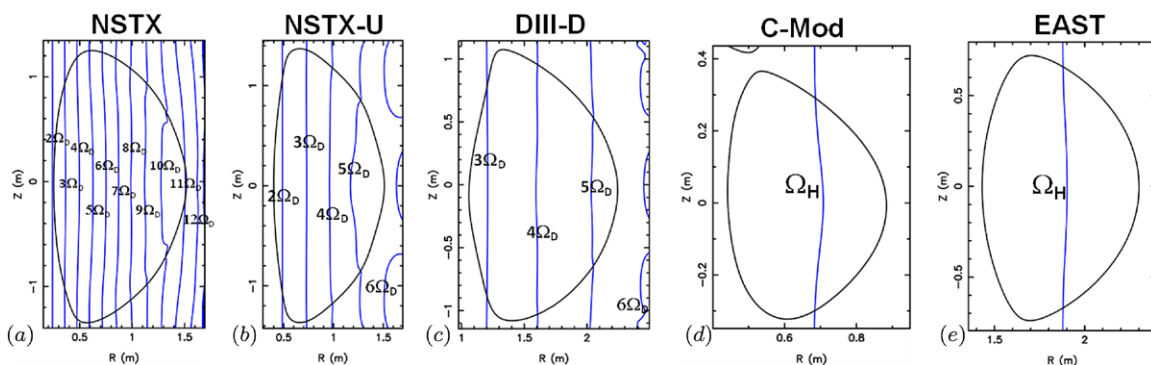


**Figure 14.** Deuterium cyclotron resonances for NSTX with  $B_T = 0.55$  T and  $\omega/2\pi = 30$  MHz (figure (a)), NSTX-U with  $B_T = 1$  T and  $\omega/2\pi = 30$  MHz (figure (b)), and DIII-D with  $B_T = 1.85$  T and  $\omega/2\pi = 60$  MHz (figure (c)). Fundamental hydrogen cyclotron resonance for Alcator C-Mod with  $B_T = 5.41$  T and  $\omega/2\pi = 80$  MHz (figure (d)) and EAST with  $B_T = 1.95$  T and  $\omega/2\pi = 27$  MHz (figure (e)).

the FW can propagate in the SOL region and large RF electric fields together with high SOL power losses have been found in the ‘standard’ NSTX-U with  $B_{T,0} = 1$  T and  $I_p = 1$  MA (see figure 5 in [24]). In figure 12 one can note that with changing the magnetic pitch angle, the large high RF field amplitude in

the SOL region is still present but the region with the strongest RF field amplitude moves down from the mid-plane as the plasma current is increased. Finally, figure 13 shows an additional case assuming a purely toroidal magnetic field (i.e.  $B_p = 0$ ) for NSTX case with  $n_\phi = -12$ . Even in this extreme

case a large amplitude RF field is found in the SOL. However, large differences occur between figure 13 and figure 2(b) in [24] (same color scale adopted), which shows the same NSTX case with the full magnetic field (i.e.  $B_p \neq 0$ ). For  $B_p = 0$ , the transition to a large total electric field in the entire SOL region appears at a larger density with respect to the case with  $B_p \neq 0$  (see also figure 3 for DIII-D). These results seem to suggest that the magnetic pitch angle plays a significant role in the behavior of the RF field and the corresponding RF losses in the SOL although it might not be a dominant effect influencing the presence of the RF field transition in the SOL.

#### 4.2. Hydrogen minority ICRH versus mid/high harmonic ICRH regimes

The main difference between the hydrogen minority ICRH and the mid/high harmonic ICRH regimes are the harmonic numbers (i.e.  $n \equiv \omega/\omega_{c,i}$ , where  $\omega_{c,i}$  is the ion cyclotron angular frequency) present in the plasma and the interaction with the minority and the majority ion species, respectively. Figure 14 shows the deuterium cyclotron resonances for NSTX (from the 2th to the 12th harmonic for  $f = 30$  MHz and  $B = 0.55$  T), NSTX-U (from the 2th to the 6th harmonic for  $f = 30$  MHz and  $B = 1$  T), and DIII-D (from the 3th to the 6th harmonic for  $f = 60$  MHz and  $B = 1.85$  T) as well as the fundamental hydrogen cyclotron resonance for Alcator C-Mod and EAST. Although differences exist in the cyclotron resonances in the core and edge plasma, there is not clear evidence in the full wave simulations, presented in this work, of a specific role of the cyclotron resonances in the SOL plasma regarding the large RF field amplitude and the RF power lost to the SOL.

## 5. Conclusions

In this paper we showed 2D AORSA full wave simulations for NSTX/NSTX-U and a sensitivity analysis on the artificial collisional damping (which was not given in [24]) employed as a proxy to study the behavior of the SOL power losses. In summary the main results from the numerical simulations are the following: (i) when evanescent waves become propagating waves in the SOL, due to higher density in front of the antenna, the power losses start to increase significantly (independent of the value of the artificial collisional damping), commensurate with the amplitude of the RF field found in the SOL; (ii) the transition to higher SOL power losses follows equation (3); and (iii) independent of the  $\nu/\omega$  value the general behavior of the SOL power losses does not change. An extension of the 2D AORSA full wave numerical analysis has been performed for ‘conventional’ tokamaks with higher aspect ratios, such as the DIII-D, Alcator C-Mod, and EAST devices, in order to estimate the behavior of the RF power losses in ‘standard’ geometry experiments with both similar and different heating regimes and compare them with NSTX/NSTX-U results. DIII-D results are found to be in agreement with the results obtained for NSTX/NSTX-U and they are also in agreement with previous experimental observations [2]. In contrast, numerical simulations for Alcator C-Mod and

EAST, which operate with ICRH in the hydrogen minority regime in a deuterium majority plasma, differ from the simulation results for NSTX/NSTX-U and DIII-D, which operate in the mid/high ICRH harmonic regime. However, the behavior of the SOL power losses in the ICRH minority regime seems more intuitive and consistent with the experiment in terms of higher antenna-plasma coupling, i.e. lower SOL power losses, with increasing SOL density. A sensitivity analysis on  $\nu/\omega$  has been presented for DIII-D, Alcator C-Mod, and EAST, indicating that the general behavior of the SOL power losses does not change varying  $\nu/\omega$ , as found for NSTX. Furthermore, a discussion of some points which might contribute to the different RF SOL losses behavior, such as (i) the pitch angle of the magnetic field; and (ii) minority heating versus mid/high harmonic regimes have been presented. The numerical simulations presented in this paper for both FW heating regimes are consistent with the corresponding experimental observations. However, further experimental studies are needed for quantitative comparison. AORSA full wave simulations will be validated with the upcoming NSTX-U campaign, with the help of a set of new coaxial Langmuir probes and an IR camera dedicated to the study of the interaction between HHFW and SOL region. Finally, improvement of the full wave code AORSA will be considered implementing a more realistic boundary condition (limiter boundary) with a 2D SOL density model ( $\rho, \theta$ ) with the aim of better understanding the behavior of the standing wave outside of the LCFS. Its application will be part of a future work.

## Acknowledgments

This material is based upon work supported by the U.S. Department of Energy, Office of Science, Office of Fusion Energy Sciences under contract numbers DE-FC02-01ER54648, DE-AC02-09CH11466, DE-AC05-00OR22725, and DE-AC02-05CH11231.

## References

- [1] Gormezano C. et al 2007 Progress in the iter physics basis chapter 6: steady state operation *Nucl. Fusion* **47** S285
- [2] Petty C.C. et al 1999 *Nucl. Fusion* **39** 1421
- [3] Biewer T.M. et al 2005 *Phys. Plasmas* **12** 056108
- [4] Wukitch S.J. et al 2007 *AIP Conf. Proc.* **933** 75
- [5] Wukitch S.J. et al 2007 *J. Nucl. Mater.* **363–5** 491
- [6] Hosea J.C. et al 2008 *Phys. Plasmas* **15** 056104
- [7] Jacquet P. et al 2011 *Nucl. Fusion* **51** 103018
- [8] Wukitch S.J. et al 2013 *Phys. Plasmas* **20** 056117
- [9] Litaudon X. et al 2013 *Nucl. Fusion* **53** 083012
- [10] Bobkov V. et al 2013 *Nucl. Fusion* **53** 093018
- [11] Wilson J.R. et al 2005 *AIP Conf. Proc.* **787** 66
- [12] Pace D.C. et al 2012 *Nucl. Fusion* **52** 063019
- [13] Antar G. et al 2014 *Nucl. Fusion* **54** 083018
- [14] Myra J.R. et al 2006 *Nucl. Fusion* **46** S455
- [15] Myra J.R. 2014 *Phys. Plasmas* **21** 022507
- [16] Ono M. et al 2000 *Nucl. Fusion* **40** 557
- [17] Phillips C.K. et al 2009 *Nucl. Fusion* **49** 075015
- [18] Taylor G. et al 2010 *Phys. Plasmas* **17** 056114
- [19] Perkins R.J. et al 2012 *Phys. Rev. Lett.* **109** 045001
- [20] Perkins R.J. et al 2013 *Nucl. Fusion* **53** 083025

- [21] Jaeger E.F. et al 2001 *Phys. Plasmas* **8** 1573
- [22] Green D.L. et al 2011 *Phys. Rev. Lett.* **107** 145001
- [23] Bertelli N. et al 2014 *AIP Conf. Proc.* **1580** 310
- [24] Bertelli N. et al 2014 *Nucl. Fusion* **54** 083004
- [25] Luxon J.L. 2002 *Nucl. Fusion* **42** 614
- [26] Greenwald M. et al 2005 *Nucl. Fusion* **45** S109
- [27] Wan B. et al 2009 *Nucl. Fusion* **49** 104011
- [28] Menard J.E. et al 2012 *Nucl. Fusion* **52** 083015
- [29] Pinsker R.I. et al 2006 *Nucl. Fusion* **46** S416
- [30] Zhang X.J. et al 2013 *Nucl. Fusion* **53** 023004
- [31] Jacquet P. et al 2012 *Nucl. Fusion* **52** 042002
- [32] James A.N. et al 2013 *Plasma Phys. Control. Fusion* **55** 125010
- [33] Jacquet P. et al 2013 *J. Nucl. Mater.* **438** S379
- [34] Ochoukov R. et al 2014 *Plasma Phys. Control. Fusion* **56** 015004
- [35] Gerhardt S.P., Andre R. and Menard J.E. 2012 *Nucl. Fusion* **52** 083020